Pressure build-up analysis in the flow regimes of the CO_2 sequestration problem

Ernestos Sarris[1*], *Elias* Gravanis[2], and *Loizos* Papaloizou[1]

[1]University of Nicosia, Department of Engineering, P.O.Box 24005, 1700, Nicosia Cyprus
[2]Cyprus University of Technology, Department of Civil Engineering and Geomatics, P.O.Box 50329, 3603, Limassol-Cyprus

Abstract. In this work we analyse theoretically and numerically the pressure build-up on the cap rock of a saline aquifer during CO_2 injection in all flow regimes. Flow regimes are specific regions of the parameter space representing the mathematical spread of the plume. The parameter space is defined in terms of the CO_2-to-brine relative mobility λ and the buoyancy parameter Γ. In addition to the known asymptotic self-similar solutions for low buoyancy regimes, we introduce two novel ones for the high buoyancy regimes via power series solutions. Explicit results for the peak pressure value on the cap, which arises in the vicinity of the well, are derived and discussed for all flow regimes. The analytical results derived are then applied for cap integrity considerations in six test cases of CO_2 geological storage from the PCOR partnership, most of which correspond to high buoyancy conditions. The validity of the self-similar solutions which are late time asymptotics, is verified with CFD numerical simulations with a commercial software. The comparison between the self-similar solutions and CFD for the pressure estimations are in excellent agreement and the self-similar solutions are valid for typical injection durations even for early times.

1 Introduction

Various observations have lead the scientific community to believe that CO_2 emitted from combustion of fossil fuels may be responsible for the global temperature increase causing adverse effects in the environment. The CO_2 emitted in the atmosphere is now regulated by laws and requires significant global investments reaching the magnitude of 1.6 trillion dollars per year to reduce emissions for the various technologies (e.g. renewables, nuclear and CCS). The technologies related with CCS are not yet fully understood and many of them are still under development. It is however, widely known that CO_2 sequestration presents many similarities with a technology utilized by the oil and gas industry during tertiary recovery also known as enhanced oil (EOR) or gas recovery (EGR) [1-3].

A good choice of reservoir rocks for storing CO_2 in the subsurface are saline aquifers. Such reservoirs are usually located deep below the surface rendering appropriate thermodynamic conditions (pressure and temperature) ensuring that the stored CO_2 will remain stable under supercritical state thereby making the CO_2 storage efficient. Furthermore, saline aquifers are also chosen due to the large storage quantities that can host subsurface. The supercritical CO_2 has a density that is significantly elevated compared with standard gas form of CO_2 and at the same time is quite smaller compared with the saline water (brine) that exists in the aquifer. Differences can reach up to 700 kg/m^3 mainly due to depth. Other parameters influencing the density include the geo-gradient, the large pressure encountered in these depths, the temperature conditions at the surface and the salinity concentration encountered in the water of the aquifer. The problem can reduce to the flow of CO_2 displacing the brine in the porous aquifer which is mostly a multi-phase flow problem in porous media. The successful solution is related to injectivity of fluids under reservoir conditions, successful CO_2 containment, formation caprock integrity and pressure build-up during long term storage [4-8].

The physical process of CO_2 sequestration into deep formations is usually described by a nearly immiscible multiphase flow of CO_2 under supercritical conditions displacing the saline fluid in the porous aquifer. The difference in their densities leads to buoyancy effects forcing the injected CO_2 to move towards the cap rock of the porous medium rather fast therefore achieving vertical gravity segregation between the CO_2 and the saline resident fluid. The CO_2 accumulates at the top of the formation (cap rock) while brine recedes at the bottom in the porous formation. Furthermore, according to the properties of these fluids, CO_2 can migrate away from the injection site (wellbore) depending on its buoyancy and mobility relative to the resident fluid. Usually, the modeling of this two-phase flow in porous media involves complete gravity segregation which is a sharp interface that separates the two fluids. According to the Dupuit approximation which is an assumption, when the time scale required for buoyant segregation is small compared to the time scale required for horizontal propagation of this interface, then

* Corresponding author: sarris.e@unic.ac.cy

it can be assumed that the CO_2 and the brine have reached pressure equilibrium in the vertical direction so that the two fluids move only horizontally. Another assumption it that the of capillary pressure can be safely assumed negligible and the miscibility between the CO_2 and the resident fluid will lead to the well-known non-linear diffusion equation that describes the dynamics of the sharp interface evolution [1, 2, 9].

Lately, research has showed that a flow regime analysis identifying the validity of asymptotic solutions in the parameter space (λ, Γ) can be constructed for this problem. Where λ is the CO2-to-brine relative mobility, and Γ is the buoyancy parameter which can be interpreted as the ratio of buoyancy to injection pressure scales, encoding the strength of buoyancy. The reported regimes I to III correspond to injection driven flows with the injected fluid being (a) highly viscous, (b) equally viscous and (c) less viscous, than the saline fluid in the aquifer. For these regimes, simple analytical solutions do exist. For regime IV, that represents the buoyancy driven flow, for which in our previous work [1] we presented a novel analytical solution in terms power series. Finally, regime V represents the transition where the forces generated by fluid injection become comparable with the forces generated by buoyancy. This regime requires numerical solution of the exact self-similar equation where no analytical solution is feasible.

In this work we briefly outline the derivation of the pressure formulas at the cap rock for all flow regimes as presented in [1] based on the fundamental work of [2] and in particular at the location next to the well, that is, the peak of the cap pressure. We also present the analytical solution derived for the Regime IV in terms of power series as well as the analytical solution of a region in the overlap of Regimes IV and V which we termed as Regime IV+ in [1], together with the respective cap pressure expressions. Regime V, which by definition requires the solution of the self-similarity equation of the problem. The solution is based on a previous work of ours [2] where the self-similar plume interface evolution was studied in detail. The non-linear self-similarity equation, first derived and discussed in [9], is indeed susceptible only to numerical solution but amounts to a far simpler and computationally economic than the one dealt with a two-phase CFD solver. Given that the self-similarity solutions are late time solutions, we set the derived cap pressure profiles against the results of a two-phase flow solver (which utilizes the volume of fluid method V.O.F. suit of methods in CFD numerical calculations [10]).

This work is organised as follows: in section 2 we present the theoretical background of the self-similar plume evolution, the flow regime asymptotic solutions and the associated pressure build-up analysis. In section 3, we describe the numerical CFD models and present and critically evaluate the findings of this research work. Finally, in section 4 we present certain conclusive remarks.

2 Theoretical Analysis

2.1 Self-similarity equation

We model the spreading of the (supercritical) CO_2 plume into a porous formation, initially saturated with brine, as an immiscible displacement problem obeying axisymmetry. The formation is assumed homogeneous and confined above and below by impermeable geological settings. It is also assumed that a sharp interface develops between the invading fluid (CO_2) and the resident brine, which are immiscible, assuming vertical equilibrium and neglecting the capillary pressure. The fluids are taken to be Newtonian, incompressible, and chemically inert, as simplifying assumptions for the theoretical analysis.

The validity of the gravity segregation (sharp interface) and vertical equilibrium was discussed in [36] based on the work of [37]. Vertical equilibrium is maintained due to the large aspect ratio of the plume, that is, its radial extent is much larger than its thickness, at the mature stage of the plume evolution. In the case under consideration the aspect ratio is roughly 100:1, leading to a negligible error of the order $(1/100)^2$, according to the estimate of [36]. The assumption that the capillarity effects are negligible implies that the fluids are solely segregated according to density. This assumption is less well founded, as capillary forces lead to non-negligible transition saturation zone that may modify the sharp interface or invalidate this simplifying assumption [38-41]. Nonetheless capillary effects are in general less important than the effects of gravity in this problem (see e.g. [42]) and we shall neglect the capillary pressure effects.

The equations governing the evolution of the CO_2-brine interface have been developed in [32] (see also [36] [43]). Let k be the intrinsic permeability of the porous medium and φ is the porosity of the formation. The mass density of the CO_2 will be denoted by $\rho_c \equiv \rho$ and that of the brine $\rho_w \equiv \rho + \Delta\rho$. The dynamic viscosity of CO_2 and brine will be denoted respectively by μ_c and μ_w. The relative permeabilities associated with the two fluids are taken to be 1 for simplicity. We should note that in real applications, the relative permeabilities differ from the value assumed for this analysis. (The maximum value of brine is 1, but for the CO_2 is rather near 0.6 as saturation cannot reach 100%). Let be the thickness of the CO_2 plume at time and distance from the well. The time-dependence of all quantities will be left understood from here on. Q is the flow rate of CO_2 injection. The formation is bounded at the top and bottom by two impermeable layers at z=0 (cap) and z=H (bed), see Fig. 1. The equation governing the evolution of the sharp interface [9] is the following:

$$\frac{\partial h}{\partial t} = \frac{1}{r}\frac{\partial}{\partial r}\left[\begin{array}{l}\dfrac{\Delta\rho g k \lambda_w}{\phi}\dfrac{\lambda h(H-h)}{\lambda h + H - h} r\dfrac{\partial h}{\partial r} + \\ + \dfrac{Q}{2\pi\phi}\dfrac{H-h}{\lambda h + H - h}\end{array}\right] \quad (1)$$

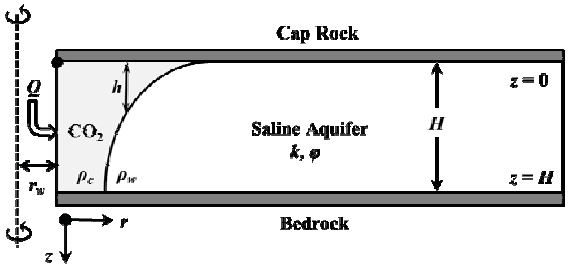

Fig. 1. Schematic of CO_2 plume spreading into the formation.

where we introduce the mobilities of the CO_2 and water, λ_c and λ_w respectively, and the mobility ratio λ (relative mobility of CO_2):

$$\lambda = \frac{\lambda_c}{\lambda_w} = \frac{\mu_w}{\mu_c} \tag{2}$$

The pressure gradients are related to the volumetric rates of each fluid, after integrating vertically the generalized Darcy law for the two-phase flow, as it is usual when vertical hydrostatic equilibrium is assumed [43, 32]. By mass conservation and vertical hydrostatic equilibrium one obtains [1]:

$$Q = -2\pi rk\left\{\begin{array}{l} h\lambda_c\left[\dfrac{\partial p_{\mathrm{cap}}(r)}{\partial r}\right] + \\ +(H-h)\lambda_w\left[\dfrac{\partial p_{\mathrm{cap}}(r)}{\partial r} - \Delta\rho g\dfrac{\partial h(r)}{\partial r}\right] \end{array}\right\} \tag{3}$$

which relates the pressure at the cap at a radial distance r from the wellbore center to the CO_2 plume thickness profile $h(r)$ as shown in Fig 1.

Defining the dimensionless plume thickness by x and the self-similarity radial distance (squared) by χ through the equations:

$$\frac{r^2}{t} = \frac{Q}{\pi\phi H}\chi, \qquad x = \frac{h}{H} \tag{4}$$

One may seek a solution of Eq. 1 of the form $h = H\,x(\chi)$. One thus obtain the self-similar equation:

$$-\chi\frac{dx}{d\chi} = \frac{d}{d\chi}\left[2\Gamma\frac{\lambda x(1-x)}{\lambda x+1-x}\chi\frac{dx}{d\chi} + \frac{1-x}{\lambda x+1-x}\right] \tag{5}$$

where Γ is the buoyancy parameter [9]:

$$\Gamma = \frac{2\pi H^2\Delta\rho g k\lambda_w}{Q} \tag{6}$$

2.2 Pressure analysis in the flow regimes

Along the saline aquifer three regions will be formed: the inner (pure CO_2) region next to the well, the two-phase i.e. interface region, and the outer (pure brine) region. There are two cases: (1) the plume profile has no trailing edge, in which case there is no pure CO_2 region and (2) the plume has a trailing edge with a dimensionless (squared) distance χ_{bed}. For cap integrity considerations, we are interested in the cap pressure at the well relatively to the cap pressure at the tip of the plume: $P = p_{\mathrm{cap}}(r_w) - p_{\mathrm{cap}}(r_{\mathrm{cap}})$. We shall call P as the injection pressure. Equation (3), along with the definitions in Equation (5) allow for the derivation of the injection pressure P [1]. In what follows we use the notation $r' = \sqrt{\chi}$. We have introduced the locations where the plume–brine interface meets the bed and the cap of the aquifer, $r_{\mathrm{cap}} = r(h=0)$ and $r_{\mathrm{bed}} = r(h=H)$. Also, $r'_{\mathrm{cap}} = r'(x=0)$ and $r'_{\mathrm{bed}} = r'(x=1)$, respectively, in dimensionless form. These correspond to the leading and trailing edges of the plume, respectively. Also, in accordance with our definition, in terms of the self-similarity coordinate, we have $\chi = (r')^2$ and $\chi_{\mathrm{cap}} = (r'_{\mathrm{cap}})^2$.

Case (2). Pressure P can be written as (details of the derivation are given in [1]):

$$\frac{P}{P_0} = \frac{1}{\lambda}\log\frac{r'_{\mathrm{bed}}}{r'_w} + \left\{\begin{array}{l} \dfrac{1}{2}\displaystyle\int_{\chi_{\mathrm{bed}}}^{\chi_{\mathrm{cap}}}\frac{d\chi}{\chi[1+(\lambda-1)x(\chi)]} + \\ \dfrac{\Gamma}{\lambda-1}\left\{-1+\dfrac{\lambda\ln\lambda}{\lambda-1}\right\} \end{array}\right\} \tag{7}$$

where we have introduced the pressure scale P_0 through which we will express the pressure in dimensionless form [1]:

$$P_0 = \frac{Q\mu_w}{2\pi kH} \tag{8}$$

Case (1). Pressure P can be written as [1]:

$$\begin{aligned} \frac{P}{P_0} = {} & \frac{1}{2}\int_{\chi_w}^{\chi_{\mathrm{cap}}}\frac{d\chi}{\chi[1+(\lambda-1)x(\chi)]} + \\ & \frac{\Gamma}{\lambda-1}\left\{-x(\chi_w) + \frac{\lambda\ln[1+(\lambda-1)x(\chi_w)]}{\lambda-1}\right\} \end{aligned} \tag{9}$$

In the previous formula we have introduced the self-similarity coordinate χ_w and radial distance r_w of the well [1]:

$$\chi_w = (r'_w)^2 = \frac{\pi\phi H}{Qt}r_w^2 \tag{10}$$

In what follows we derive the injection pressure P for the different flow regimes [11]. We also introduce a new flow regime and the associated injection pressure formula.

Regime I: $\Gamma<<1$ and $\lambda< 1$ (low buoyancy, low CO_2 mobility). The plume profile is given by [1]:

$$x = \frac{1-\lambda}{2\Gamma\lambda}(1-\chi)+\frac{1}{2} \tag{11}$$

The injection pressure P from Eq. 9 for this regime explicitly reads:

$$\frac{P_I}{P_0} = \frac{1}{\lambda}\ln\frac{\sqrt{1-\frac{\lambda\Gamma}{1-\lambda}}}{r_w'} + \frac{\lambda\Gamma\ln\left(\frac{1-\lambda-\lambda\Gamma}{\lambda(1-(1-\Gamma)\lambda)}\right)}{(1-\lambda)^2-\lambda\Gamma(\lambda+2)} + \\ + \frac{\Gamma}{\lambda-1}\{-1+\frac{\lambda\ln\lambda}{\lambda-1}\} \tag{12}$$

Regime II: $\Gamma<<1$ and $\lambda= 1$ (low buoyancy, unit CO_2 mobility) [1].

$$x = \frac{1}{2\sqrt{\Gamma}}(1-\chi)+\frac{1}{2} \tag{13}$$

$$\frac{P_{II}}{P_0} = \ln\frac{1+\sqrt{\Gamma}}{r_w'}+\frac{\Gamma}{2} \tag{14}$$

Regime III: $\Gamma<<1$ and $\lambda>1$ (low buoyancy, high CO_2 mobility) [1]:

$$x = \frac{\sqrt{(\lambda/\chi)}-1}{\lambda-1} \tag{15}$$

$$\frac{P_{III}}{P_0} = \frac{1}{\lambda}\ln\frac{1}{r_w'\sqrt{\lambda}}+1-\frac{1}{\lambda}+\frac{\Gamma}{\lambda-1}\{-1+\frac{\lambda\ln\lambda}{\lambda-1}\} \tag{16}$$

Regime IV: $\Gamma>>1$ (high buoyancy). This region of the parameter space is specified as shown in Fig. 3. Roughly speaking one may say that it corresponds to cases where $\Gamma\lambda$ and Γ/λ are bounded from below by order 1 constants, for large and small λ, respectively.

For this regime an analytical solution in terms of power series was given in [1]. In particular, the self-similarity Eq. 5 in the large buoyancy limit takes the form [11, 12]:

$$4(yff')'+yf'=0 \tag{17}$$

where

$$y=\frac{\chi}{\chi_{\text{cap}}},\quad f=\frac{\Gamma\lambda}{2\chi_{\text{cap}}}x \tag{18}$$

with the boundary conditions $f(1^-)=0,\ f'(1^-)=-1/4$. The first condition expresses the zero plume thickness, while the first derivative condition is imposed by the equation itself upon requiring that the solution is expressible in power series. Eq. 17 can be solved in terms of power series [1] and the injection pressure for this regime is given by

$$\frac{P_{IV}}{P_0} = \frac{1}{2}\ln\frac{\chi_{\text{cap}}}{\chi_w}+\frac{2\chi_{\text{cap}}}{\lambda}f(\frac{\chi_w}{\chi_{\text{cap}}}) \tag{19}$$

Regime V: The intermediate buoyancy is shown in Fig. 3. It corresponds to the cases where a numerical solution of the self-similarity Eq. 5 is necessary. Injection pressure may be calculated by Eq. 7 or Eq. 9, depending on the conditions of the problem.

Regime IV+: The solution presented for Regime IV can be modified to hold well on a region on the overlap of Regime IV and Regime V, as given in Fig. 3. Put differently, one may find a solution for regime V near its boundary with Regime IV.

In [1] it was shown that upon replacing

$$\Gamma\to\frac{\Gamma}{\lambda-1} \tag{20}$$

in the solution of the regime IV one obtains a solution that holds well roughly in a region on the border between regime IV and V which we call regime IV+ and can be described by $\Gamma<<\lambda^2$.

3 Numerical Modelling and Results

Owing to the inherent nonlinearities in the multiphase flow regimes, the immiscible displacement of CO_2 displacing saline water from the porous formation, holds special challenges in the modeling because of the interaction of the fluids with the porous formation. Closed form analytical solutions are rare and apply under specialized or ideal conditions, thus computational modeling proof to provide valuable tools for investigating the dynamics of the CO_2 front invading the porous medium and the associated pressure build-up. The numerical computations were carried out in Ansys-Fluent, a nonlinear CFD code [10].

The considered domain was discretized to (5000×30) m so as to ensure vertical equilibrium and the gravity segregation assumption to hold. The wellbore location is at the left corner. The wellbore radius is set to $r_w = 0.15$ m. Given the large horizontal dimensions of the formation, the size of the wellbore radius becomes negligible and its effects can be ignored. The model is axisymmetric and in agreement with the theoretical derivations of section 2. The injection of the CO_2 performed at the wellbore constitutes the inlet boundary condition. To simulate the impermeable rock layers above and below the aquifer, no flow wall boundary conditions were considered at these locations. Finally, the outlet boundary condition of zero gauge pressure was imposed in order to ensure flow towards the outer

boundary of the models. A sufficient fine mesh around the wellbore and in the vicinity of the caprock was used, so that to effectively track the fine changes at the interface of the two fluids and to resolve numerical instabilities arising around the interface which results in pressure changes in the various flow regimes of the problem [1, 2].

The results from the simulations are based on 48k grid cells. The grid spacing in the radial direction starts with a spacing of 0.96 m and increases geometrically by a factor of 1.0038. Totally, there were 800 grid cells in that directions. The grid spacing in the vertical direction starts with a spacing of 0.145 m at the cap and increases geometrically with a factor of 1.0364. Totally, includes 60 grid cells in the vertical direction. Roughly 1/3 of the mesh is used near the cap in order to capture fine physical changes in the interface evolution and the associated pressure build-up. The calculations were carried out in Ansys-Fluent, a nonlinear CFD code suit of programs. The usual 8-node tetrahedral cell elements were used to model the fluid flow in the aquifer and the interface evolution process. The computation of the fluid diffusion in the porous domain and the interface evolution process with the associated pressure build-up is performed by the displacement of the dense fluid by the less dense (CO_2) in the cells center [1, 2]. Figure 2 presents the details of the considered domain with the wellbore location, grid spacing/size used in the numerical modeling while the color map shows the two fluid phases.

The analysis that follows presents the application of the mathematical derivations of section 2 with the case studies of reference [13]. Namely, these case cases are two large saline aquifers being used as CO_2 sequestration sites which are sandstone and limestone of formations. For abbreviation purposes, the sandstone formations were named as (Cretaceous A, B, C) while the carbonate formations were named as (Madison A, B, C). The flow regimes as described in section 2 are identified on the (λ, Γ) parameter space of each of the six cases. The calculations for the (λ,Γ) and their corresponding flow regimes are presented in Table 1.

Table 1. Madison and Cretaceous injection pressure estimate

Madison group			
Variables	MA	MB	MC
Γ	**6.6**	**0.64**	**4.8**
λ	**11.7**	**30.4**	**15.4**
Regime	**V**	**III**	**V**
$P_{\text{self-similar}}$ [MPa]	1.21	2.81	0.94
$P_{\text{analytical}}$ [MPa]	-	1.31	-
$P_{\text{M. et al. 2009}}$ [MPa]	1.46	3.74	1.47
Cretaceous group			
Variables	CA	CB	CC
Γ	**15.1**	**79.6**	**51.3**
λ	**20.8**	**26.0**	**13.5**
Regime	**V**	**IV+**	**IV+**
$P_{\text{self-similar}}$ [MPa]	1.38	0.46	0.93
$P_{\text{analytical}}$ [MPa]	-	0.45	0.925
$P_{\text{M. et al. 2009}}$ [MPa]	1.21	0.25	0.54

Fig. 3 shows pictorially the mapping in flow parameter space the six cases considered with the following abbreviations: Madison B maps in the flow regime III, Madison A, C and Cretaceous A fall into Regime V, while Cretaceous B and C fall on what we have called Regime IV+. Fig. 3 shows that the conditions of all formations correspond to high buoyancy except of the Madison B case. This mapping renders virtually the pressure calculation of [6, 13] inapplicable for these cases. It may then be no surprise that, as it can be seen in Table 1, the injection pressure for the high buoyancy cases of the Cretaceous A, B, C formations is consistently higher when calculated through the self-similar solutions compared with the pressure calculation of [6, 13]. This occurs in spite of the different mobility from case to case, and the inclusion of the compressibility and inertial effects considered in the work of [6, 13]. This finding is also shown in Fig. 4, through the indicated curves, in terms of the injection pressure scaled by P_0 (Eq.8) as a function of the buoyancy parameter Γ. That implies that the high buoyancy effects are not negligible compared to the compressibility of inertial effects.

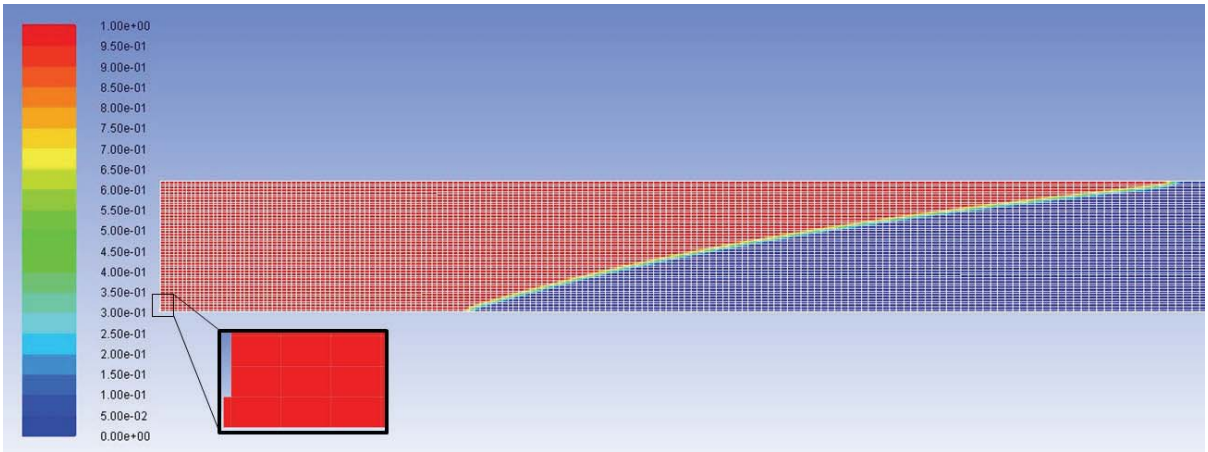

Fig. 2. Illustration of the domain with the wellbore location, grid spacing and size. Color maps show the CO_2 and brine phases in fractions of volume.

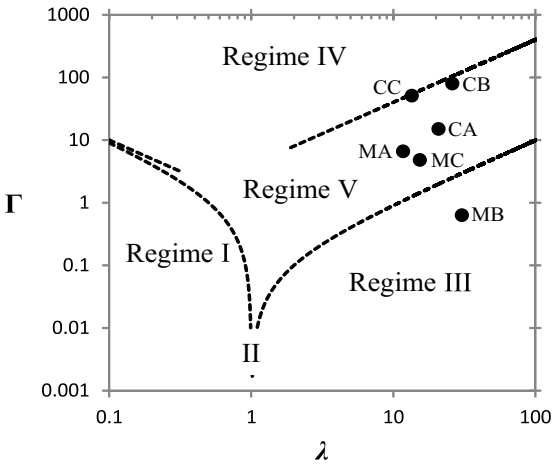

Fig. 3. The six injection sites (C: Cretaceous; M: Madison) and their mapping in the flow regime parameter space (λ,Γ).

Fig. 4 includes the results of the application of the analytical solutions presented in section 2. The outcomes of the analytical solutions presented in this research work are shown with the cross symbols. We see that the Regime IV+ cases, which happen to be the highest buoyancy ones, reproduce quite well the results of the numerical solutions of the exact self-similar equation (eq. 5). On the other hand, the analytical solution of the low buoyancy case (Regime III) deviates significantly from the results of the self-similar equation. The main reason is that the low buoyancy asymptotic solution actually corresponds to negligible buoyancy and is decently accurate only for Γ much smaller than 1.

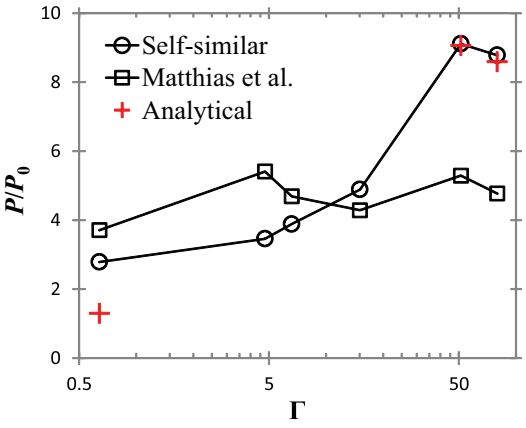

Fig. 4. Comparison of scaled injection pressures

4 Discussion and Conclusions

In this work we analyzed in detail the pressure build-up at the cap rock in the various flow regimes arising in the CO_2 sequestration problem. The aim was to understand the influence of the pressure that is applied at the cap rock during CO_2 injection for rock integrity considerations. We presented mathematical solutions for the pressure build-up for all flow regimes (where feasible) and applied them to aquifers test cases in order to check their applicability for cap rock integrity. Additionally, to the known asymptotic solutions of Regimes I, II, III we have introduced two novel analytical solutions, one applying to Regime IV and the second to an overlap between Regime IV and V, which we named Regime IV+. The latter regimes corresponds to high buoyancy and mobility conditions and they are rather important in practice. We showed that three of these test cases map into the Regime V, where the numerical solution of the exact self-similar equation (eq.5) finds excellent application. Furthermore, two other test cases map into Regime IV+ and the associated analytical solution was utilized for the pressure estimation in the formation.

The main findings of this work can be summarized as follows: (A) we derived pressure build-up relations for all flow regimes (I-V). (B) We provided new explicit analytical solutions for regimes IV and IV+. (C) We showed that the applicability of the self-similarity equation and its flow regime asymptotic solutions are applicable as early as the buoyancy time scale verified with CFD numerical simulations. (D) The self-similar and CFD models are capable for providing excellent estimates for the pressure build-up for a wide range of buoyancy parameters and fluid mobilities.

References

1. E. Sarris, E. Gravanis, “Flow regime analysis of the pressure build-up during CO_2 injection in saturated porous rock formations”. Energies, **12**(15), 2972 (2019)
2. E. Sarris, E. Gravanis, P. Papanastasiou, “Investigation of self-similar interface evolution in carbon dioxide sequestration in saline aquifers”. Transp. Porous Media **103**, 341-359 (2014)
3. P. Papanastasiou, E. Papamichos, C. Atkinson, “On the risk of hydraulic fracturing in CO_2 geological storage”. Int. J. Num. An. Meth. Geomech. **40**, 1472-1484 (2016)
4. B. Guo, Z. Zheng, K.W. Bandilla, M.A. Celia, H.A. Stone, “Flow regime analysis for geologic CO_2 sequestration and other subsurface fluid injections”. Int. J. Greenh. Gas Control **53**, 284-291 (2016)
5. A. Raza, R. Gholami, R. Rezaee, V. Rasouli, M. Rabiei, “Significant aspects of carbon capture and storage–A review”. Petroleum (2018)
6. S.A. Mathias, P.E. Hardisty, M.R. Trudell, R.W. Zimmerman, “Approximate solutions for pressure build-up during CO_2 injection in brine aquifers”. Transp. Porous Media **79**, 265-284 (2009)
7. S. Gheibi, V. Vilarrasa, R.M. Holt, “Numerical analysis of mixed-mode rupture propagation of faults in reservoir-caprock system in CO_2 storage”. Int. J. Greenh. Gas Control **71**, 46-61 (2018)
8. D. Hui, Y. Pan, P. Luo, Y. Zhang, L. Sun, C. Lin, “Effect of supercritical CO_2 exposure on the high-

pressure CO_2 adsorption performance of shales". Fuel **247**, 57-66 (2019)

9. J.M Nordbotten, M.A. Celia, "Similarity solutions for fluid injection into confined aquifers". J. Fluid Mech. **561**, 307-327 (2006)
10. Ansys, *Ansys-Fluent User Manual* (version 14, PA, USA, 2014)
11. B. Guo, Z. Zheng, M.A. Celia, H.A. Stone, "Axisymmetric flows from fluid injection into a confined porous medium". Phys. Fluids **28**, 1-22 (2016)
12. Z. Zheng, B. Guo, I. Christov, M.A. Celia, H.A. Stone, "Flow regimes for fluid injection into a confined porous medium". J. Fluid Mech. **767**, 881-909 (2016)
13. S.A. Mathias, P.E. Hardisty, M.R. Trudell, R.W. Zimmerman, "Screening and selection of sites for CO2 sequestration based on pressure build-up". Int. J. Greenh. Gas Control **3**, 577-585 (2009)